Available online at www.CivileJournal.org

Civil Engineering Journal

(E-ISSN: 2476-3055; ISSN: 2676-6957)

Vol. 11, No. 08, August, 2025

Inelastic Response of Fixed and Flexible Foundation of Structure Under Seismic Excitations Generated Deterministically

Pranowo [1*], Widodo Pawirodikromo [1], Lalu Makrup [1], Yunalia Muntafi [1]

[1] *Department of Civil Engineering, Universitas Islam Indonesia, Yogyakarta, Indonesia.*

Received 07 May 2025; Revised 04 July 2025; Accepted 11 July 2025; Published 01 August 2025

Abstract

Researchers performed inelastic dynamic analysis on simulated ground motion while accounting for foundation flexibility in the specific area of Yogyakarta. The closest fault source to the building site is the Opak Fault, situated 2.1 kilometers from the structure. The closeness to the fault source, which suggests an exceedingly high earthquake magnitude, prompted the use of deterministic analysis. Deterministic analysis used five Ground Motion Prediction Equations (GMPEs): Campbell-Bozorgnia (2006), Sadigh et al. (1997), Ciao-Youngs (2008), Zhao et al. (2006), and Kanno et al. (2006), while the flexibility of the foundation was evaluated using the formula proposed by Novak (1989). The analysis results show that the vibration period that occurs on the flexible support is 2.8 seconds, while on the fixed support it is 2.4 seconds. Deflections and drift ratios in structures with fixed support and high-frequency content are greater, but in beam curvature the results show the opposite, namely, low-frequency content produces larger curvature values. The damage index on the fixed support and high-frequency content is greater than the others. Not much research has looked into the results of inelastic response analysis that includes hysteretic loop outputs and damage indices, making this a new area of study.

Keywords: Inelastic Dynamic Analysis; Foundation Flexibility; Deterministic Seismic Evaluation; Damage Index.

1. Introduction

Earthquakes occur due to the movement of the earth's plates (crust). The frequency of an area can be estimated based on the category and size of earthquakes experienced. Buildings in earthquake-prone areas must be able to withstand earthquakes in order to minimize the harmful effects. To determine whether a building requires further analysis of its resilience, civil engineers must be able to design structures that can withstand earthquakes.

The earthquake that shook Yogyakarta on 27 May 2006 still left a deep trauma for the people of Yogyakarta and its surroundings. The Indian-Australian plate and the Eurasian plate collided, triggering the Yogyakarta earthquake. Eurasian plate. The earthquake was located at coordinates of 8.03 LS and 110.32 BT, with a depth of 2 kilometers, and the recorded magnitude was 5.9 SR with a vibration time of approximately 57 seconds. It was reported that the Yogyakarta earthquake claimed 5,778 lives and severely injured as many as 37,883 [1]. Most of the victims were caused by being buried by buildings or materials. The Yogyakarta earthquake resulted in severe damage to 96,790 buildings, moderate damage to 117,075 buildings, and minor damage to as many as 156,971 buildings. Damaged buildings indicate that the quality of building materials is not sufficient.

* Corresponding author: omprans@yahoo.com; 885110106@uii.ac.id

http://dx.doi.org/10.28991/CEJ-2025-011-08-024

An earthquake hazard analysis is necessary to prevent an earthquake from damaging a building structure. There are several approaches to synthetic ground motion for analysis; in this study, a deterministic method is used to create artificial ground motion time history. Deterministic Seismic Hazard Analysis (DSHA), a method widely used in the early periods of seismic hazard calculations [2]. The basic concept of DSHA is to determine ground motion parameters using the maximum earthquake magnitude and the distance of the earthquake source closest to the observation point.

Two methodologies are available for performing Seismic Hazard Analysis (SHA): deterministic and probabilistic. When the earthquake source is clearly identifiable, like a fault or subduction zone, we employ the DSHA approach. DSHA utilizes the greatest earthquake magnitude and the nearest earthquake source distance from the observation station. Typically, structures with significant hazard potential employ this technique to assess seismic acceleration. While this method makes it easier to guess the worst-case scenario, it doesn't take into account how likely it is that an earthquake will happen or how many other unknowns might affect the situation.

Improved methods in structural analysis are to take into account the use of soil structure (Soil Structure Interaction). Interaction has been developed in recent decades, and to obtain a solution, two approaches—impedance continuum or discrete numerical—methods can be used by considering the *coupling* effect between the soil structure of the foundation and the building structure into a structural system as a whole [3]. This will be closer to reality, and structural analysis can estimate the safety of the structure. Basically, the factor of safety can be reduced when the results show excessive safety; this can optimize construction costs.

Widodo [4] discusses the response of hysteretic energy structures and damage indices, addressing the normalization of hysteretic energy and its role in damage indices for single-degree-of-freedom structures that exhibit inelastic response during earthquakes. However, this study employs a single degree of freedom analysis, whereas high-rise building structures possess multiple degrees of freedom.

Zhang & Far [5], in his study, used a soil-foundation-structure model developed in finite element software and verified through shake table testing to critically examine the effects of SSI on tall buildings. The results showed that with an increase in foundation rotation, inter-story drift increased, and base shear decreased. In general, SSI increases inter-story drift, indicating the detrimental impact of SSI. However, regarding base shear forces, SSI has a beneficial effect as it reduces these forces, thereby decreasing the internal forces acting on beam and column elements. In this study, pile-raft foundations and regular building plans were used, and no ground motion was selected, considering frequency content.

Bradley [6] explains the deterministic limit considerations for maximum ground motion levels in earthquake design codes and standards. The fundamental reason for ground motion levels that are ‘well above average’ (for certain earthquake scenarios) is common in regions with high seismicity. This information is crucial for ensuring that structures can withstand the forces generated by significant seismic events. As a result, engineers and architects must incorporate these higher ground motion levels into their designs to enhance safety and resilience in earthquake-prone areas. In this research, by using the 5 GMPE formula and taking the average, the expected design ground motion value is neither too high nor too low, and the target spectra MCEr is used as the boundary for design ground motion.

Panowo et al. [7] studied the magnitude of earthquakes near the Opak fault using a probabilistic method, showing a deaggregation result of a potential magnitude of 5.8 Mw, meaning that the resulting displacement response is still within acceptable limits. In this study, the earthquake scenario based on PuSGeN 2022 is 6.6 Mw, which indicates a higher potential for ground shaking and displacement response. This scenario points out that there must be enhanced preparedness and resilience measures in the region to mitigate the risks associated with such seismic events.

Ricci et al. [8] investigated the new application of Neo-Deterministic Seismic Hazard Assessment (NDSHA) for earthquake hazard assessment in open fields, specifically in the city center of Chieti (Abruzzo, Italy). The results were compared with those obtained using the AlgoShake2D Finite Element Method (hereinafter referred to as FEM) in the same area. Both methods utilize the dynamic behavior of viscoelastic rock and soil. Additionally, non-linear analysis was conducted using the FEM method. Some potential complexities of earthquake sources indicate that higher amplification than FEM should be considered when more realistic simulations are available. Considering the complexity of real earthquakes and based on the principle of caution, it is reasonable to recommend routinely using NDSHA. Since the Neo-Deterministic Seismic Hazard Assessment (NDSHA) analysis is still relatively new and not yet available, this study uses the five GMPE formula, which will be explained below.

Many researchers have developed structural analysis for inelastic conditions over time, recognizing its importance. Researchers have applied several methods to design building structures or other structures with inelastic conditions. Large loads, like earthquake forces, tend to deform a structure to its inelastic limit. Therefore, we need to design building structures in earthquake-prone areas to account for their inelastic responses. The current problem is that large earthquake records in the form of time history in Indonesia are not available and are difficult to access openly to the public, so one of the objectives of this research is to explore digital data of earthquake records in Indonesia to be developed into an artificial earthquake record (Artificial Ground Motion Time History). Based on prior research, it is intriguing to explore the inelastic performance of high-rise buildings in response to deterministically developed ground motion while also considering the flexibility of the foundation.

Structure of multi-storey building is evaluated in the study build upon earthquake acceleration time history of ground motion that developed by Deterministic Seismic Hazard Analysis (DSHA). The research location is a point with global coordinates, namely - 7°51'40"S latitude; 110°23'19"E longitude. The coordinate is site of Building in Yogyakarta close to the Opak fault. The building to be analysed can be seen in Figure 1.

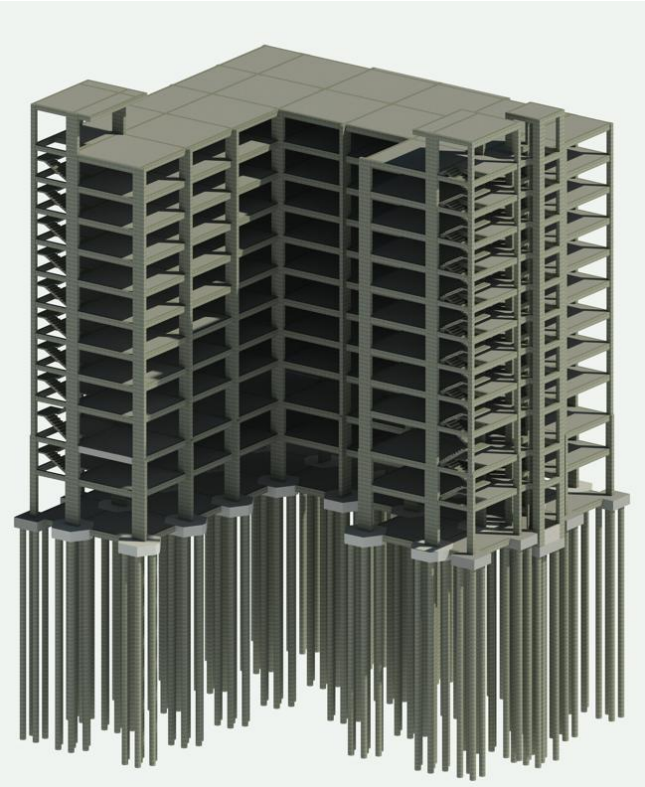

Figure 1. 3-dimensional Structure model

2. Research Methodology

This research methodology provides a concise overview of the process for obtaining artificial earthquake vibrations and foundation parameters (stiffness and damping), which will be inputted into the Ruaumoko 3D program to obtain the inelastic response of the building structure. The existing research has not addressed the gaps identified by previous studies. The initial phase of the study entailed the collection of data pertaining to tall structures in Yogyakarta. This included soil investigation data, planning drawings, and building site coordinates. The second stage of the methodology entailed the modeling of the building structure using the Ruaumoko 3D Program. This involved the input of relevant parameters, including the dimensions of the structural elements, the number of floors, the height of the building, and the operational loads. The third stage involves generating artificial earthquakes using deterministic methods, which are represented in the form of time histories, to simulate vibrations in tall buildings. The fourth stage is to obtain the foundation parameters (stiffness and damping), and the final stage is to analyze the Ruaumoko 3D program with the aforementioned input data to obtain the building response output. The Ruaumoko 3D software was used because the analysis was inelastic and the output was expected to describe the condition of the frame that had entered the inelastic level. The advantages of the Ruaumoko program are outputs that are not found in other programs, such as element stiffness history and element hysteretic loops, for which the hysteretic loop model can be selected.

Figure 2 provides a brief illustration of the process.

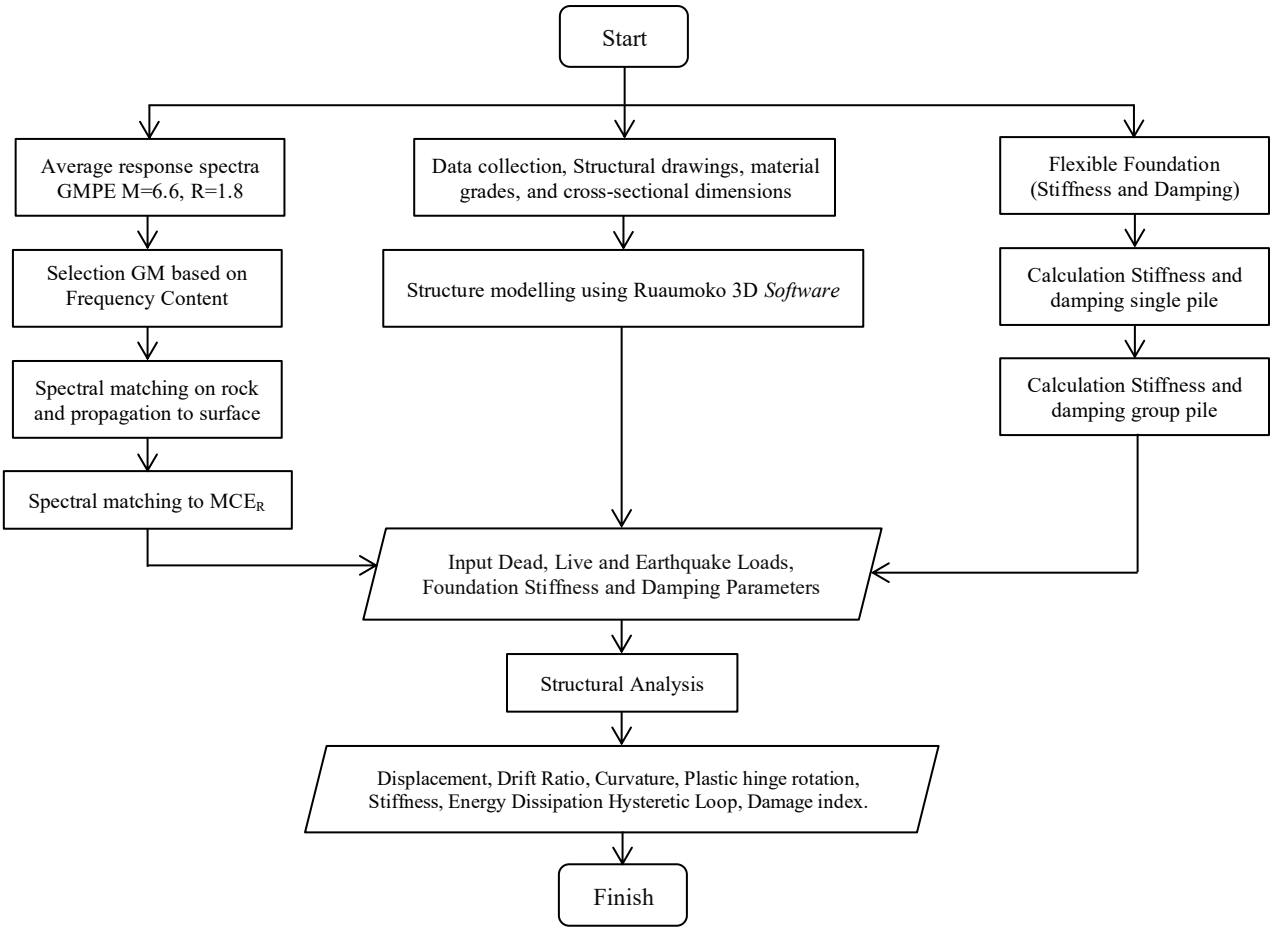

Figure 2. Research Flowchart

3. Deterministic Seismic Hazard Analysis

The development of earthquake ground motion by probabilistic procedures has been carried out by many experts. Another procedure for developing earthquake ground motion is a deterministic seismic hazard analysis. To develop a deterministic earthquake, ground motion is used as a basis for the Ground Motion Prediction Equation (GMPE). There are quite a number of GMPEs developed by experts, but in this study only Five GMPEs were used as a reference to accommodate the causes of uncertainty by using one GMPE. Because what is calculated or developed is the ground motion in the soil, the GMPE used is the GMPE of soil sites. The computational result of each GPME is the response spectrum of the bedrock. In this study, Five GMPEs will be used, namely Campbel-Borzognia (2006) [9], Sadigh et al. (1997) [10], Ciao-Youngs (2008) [11], Zhao et al (2006) [12] and Kanno et al. (2006) [13]. Why are these Five GMPEs used in research, because these five equations have input data that can still be found in Indonesia. The average value of the response spectra of the five GMPEs above will be used as a target spectrum to develop an Artificial Ground Motion Time History. The mathematical equations of Campbel-Borzognia (2006) [9], Sadigh et al. (1997) [10], Ciao-Youngs (2008) [11], Zhao et al (2006) [12] and Kanno et al. (2006) [13] are presented below:

3.1. Campbell & Bozorgnia Equation (2006)

The equation is:

$$\ln y = f_{mag} + f_{dis} + f_{flt} + f_{hng} + f_{site} + f_{sed} \quad (1)$$

In this mode, the magnitude (M), the distance to the top of the coseismic fault rupture (R_{rup}), the effect of faulting, including buried reverse faulting (FRV) and normal faulting (FNM), the depth measured from the surface to the top of the coseismic fault rupture (Z_{Tor}), fault dip (δ), depth in the crossing seismic column, which consists of shallow seismic and 3-D effect basin (Z25), effect hanging wall, site response in terms of VS30 function, and average shear wave velocity at the top 30 meters of the site soil profile (VS30). This mode calculates the VS30 value in soil to be approximately 269 m/s. The mean value of fourth GMPE above is utilized to develop the target spectrum that used in spectral matching process.

3.2. Sadigh Equation (1997)

Equation for rock site:

$$\ln Y = C_1 + C_2 M + C_3 (8.5 - M)^{2.5} + C_4 \ln[R_{rup} + \exp(C_5 + C_6 M)] + C_7 \ln[R_{rup} + 2) \quad (2)$$

Equation for soil site:

$$\ln y = C_1 + C_2 M + C_3 \ln[R_{rup} + C_4 e^{C5 M})] + C_6 + C_7 (8.5 - M)^{2.5} \quad (3)$$

where, y = spectral acceleration, M = earthquake magnitude (M = 4 to 8), R_{rup} = rupture distance (R_{rup} = 0 to 100 km), and regression coefficients C_1 to C_7.

3.3. Chiou-Young NGA Equation (2008)

The Equation is:

$$\ln(SA_{1130ij}) = c_1 + c_{1a} F_{RVi} + c_{1b} F_{NMi} + c_7(Z_{TORi} - 4) + c_2(M_i - 6) + [(c_2 + c_3)/ c_n] \ln[1 + \exp\{c_n(c_M - M_i)\}] + c_4 \ln[R_{RUPij} + c_5 \cosh\{c_6(M_i - c_{HM}, 0)_{max}\}] (c_{4a} - c_4) ln \sqrt{R^2_{rupij} + c^2_{RB}} + [c_{\gamma 1} + c_{\gamma 2}/\cosh\{(M_i - c_{\gamma 3}, 0)_{max})] R_{RUPij} + c_9 \cos^2\delta \tanh(R_{RUPij}/2) \tan^{-1}[W_i \cos \delta_i/2((Z_{TORi} + 1)] 1/(\pi/2) [1 - R_{JBij}/(R_{JBij} - 0.001)] + \tau z_i \quad (4)$$

$$\ln(SA_{ij}) = \ln(SA_{1130ij}) + \phi_1 [\ln(V_{S30ij}/1130), 0]min + \phi_2 [\exp\{\phi_2 ((V_{S30ij}, 1130)_{min} - 360)\} - \exp\{\phi_2(1130-360)\}] \ln[(SA_{1130ij}) + \phi_4)/ \phi_4] + \sigma z_{ij} \quad (5)$$

with R_{RUP} is the closest distance to rupture area (km), R_{JB} is Joiner-Boor distance (km), δ is rupture dip, $0W$ is rupture width (km), Z_{TOR} is top rupture depth (km), F_{RV} is 1 for $30^0 \le \lambda \le 150^0$ and F_{RV} is 0 other slip mechanism (reverse and reverse-oblique), F_{NM} = 1 for $-120^0 \le \lambda \le -60^0$ and F_{NM} = 0 for other slip mechanism (normal and normal-oblique), λ is rake angle, V_{S30} is soil shear wave velocity for 30 m highest soil depth in m/s, τ is standard error for inter-event, σ = standard error for intra-event.

The GMPE of Chiou-Youngs NGA 2006 should be used only for predictor variable in range:

$4 \le \mathbf{M} \le 8.5$ for strike-slip earthquake;

$4 \le \mathbf{M} \le 8.0$ for reverse slip and normal slip;

$0 \le R_{RUP} \le 200$ km;

$150 \le V_{S30} \le 1500$.

3.4. Zhao et al. Equation (2006)

The Equation is:

$$\ln(y_{ij}) = a M_{wi} + b x_{ij} - \ln(r_{ij}) + e (h - h_c) \delta_h + F_R + S_I + S_S + S_{SL} \ln(x_{ij}) + C_k + \xi_{ij} + \eta_{ij} \quad (6)$$

$$r_{ij} = x_{ij} + c \exp(d M_{wi}) \quad (7)$$

with y is PGA or spectral acceleration for 5% dumping ratio (cm/dt^2), T is spectral periods, Mw is magnitude moment, x = source distance (km), h is focal depth (km), and F_R is reverse-fault parameter, a, b, c, d, e, C_k, F_R, S_I, S_S, S_{SL} are coefficients that can be found by regression analysis, x is the closest distance to rupture zone for the fault, transform fault sources and for the source of subduction zones and fault transform, and subduction zones. For the other sources then x is the hypocenter distance.

3.5. Kanno Equation (2006)

The Equation is:

$$\log y = a_1 M + b_2 R_{RUP} - \log(R_{RUP} + c_1 + c_4 10^{0.5 M}) + p \log V_{S30} + q \quad (8)$$

Equation 8 gives the result y in cm/s^2. If y is in the acceleration due to gravity, then Equation 8 turns into equation 9.

$$\ln y = \ln(10) \log y - \ln(100g) \quad (9)$$

where, y = ground motion parameter, M = earthquake magnitude, R_{rup} = rupture distance, a_1 , b_2 , c_1 , c_4 , p and q are regression coefficients.

4. Artificial Time History

Spectral matching is a procedure to convert an earthquake acceleration time history to be a new time history, based on a known target spectrum, Nikolaou [14]. To perform the spectral matching is utilized SEISMOMATCH computer program to convert the time history of measurement result to be a new time history.

4.1. Target Spectrum

For the deterministic seismic hazard analysis, the ground motion is developed build upon the ground motion prediction equation based on PuSGen (2022) [15] with M = 6.6 and R=2 km. The target spectrum is developed based on GMPE response spectra of Campbel-Borzognia (2006) [9], Sadigh et al. (1997) [10], Chiou & Young (2008) [11], Zhao et al. (2006) [12] and Kanno et al. (2006) [13]. The study site Building with coordinate (7°51'40"S; 110°23'19"E) and epicenter coordinate (7°52'15"S; 110°24'09"E) Figure 3-a delineates the position of the special province of Yogyakarta on the map of Java Island, whereas Figure 3-b provides a more detailed depiction of the observation area surrounding the of Yogyakarta special province.

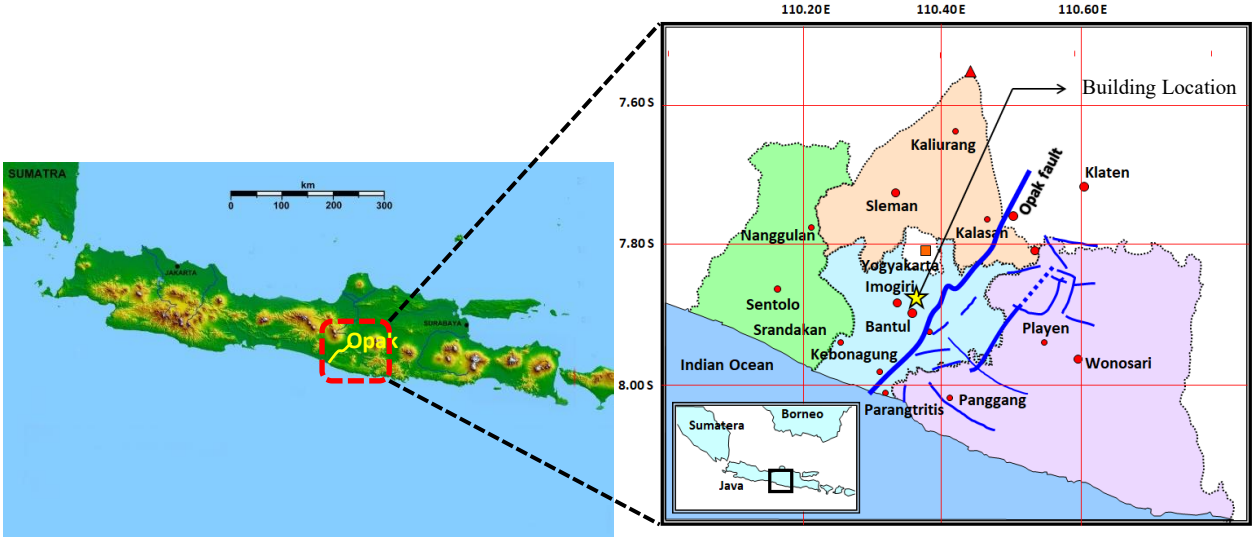

(a) Java Island *(b) Building Site*

Figure 3. Java island and Building Site in Yogyakarta Special Province (YSP)

The epicenter points and the site of Building of point it has been computed the epicenter distance R_{EPI} = 2 km. With the Equation 10 of Well & Coppersmith [16] it has been calculated the rupture length, L = 21.5774 km of the Yogyakarta earthquake.

$$\log L = 0.69M - 3.22 \quad (10)$$

From the epicenter distance, R_{EPI} = 2 km, the rupture length, L = 21.5774 km and depth of sediment deposit is assumed 100 m is calculated rupture distance R_{RUP} = 2 km and Joiner-Boore distance R_{JB} = 1.3225 km. With the four parameters M = 6.6, R_{RUP} = 2 km, R_{JB} = 1.322 km, Vs_{30} = 760 m/s and others are calculated the five GMPE response spectrum. Result of the GMPE response spectrum in the Figures 4 below.

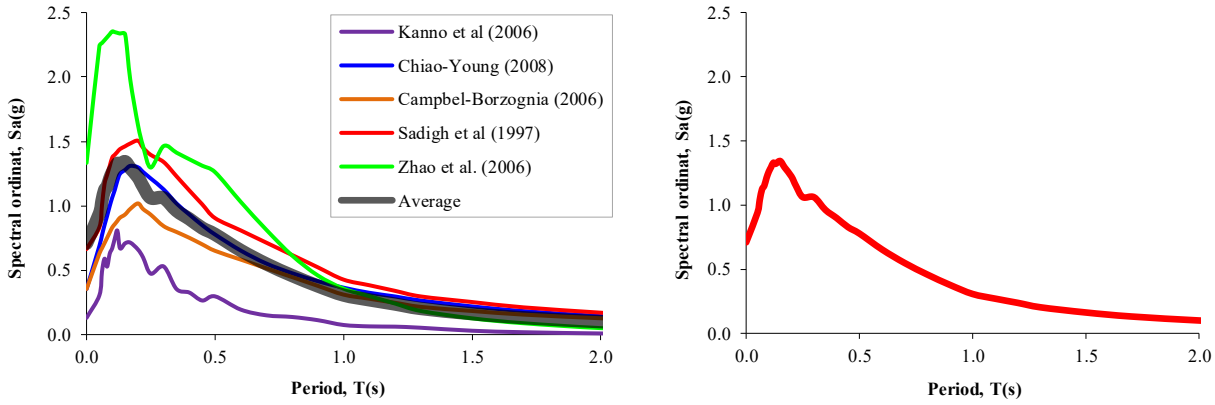

(a) Response spectra based on GMPE **(b) Average response spectra**

Figure 4. GMPE response spectra

From the five GMPE response spectrum above (Figure 4-a) is calculated the mean GMPE response spectrum and calculation result of the mean GMPE response spectrum is in the Figure 4-b.

4.2. Original Time History

In determining the ground motion for analysis based on the scenario M = 6.6 and R = 2 Km, the type of frequency is used as data representing the ground motion conditions under review.

Researchers have used the A/V ratio as an empirical metric to evaluate the frequency content of ground motion and categorize ground motion suites for nonlinear time history investigations of structures. The peak ground ratio, A/V, has been utilized to estimate the frequency content of seismic waves [17]. Tso et al. [18] classified ground motions into three types and examined their seismological importance. A study by Sawada et al. [19] found that low A/V ratios are a sign of earthquakes with low main frequencies, broad response spectra, long durations, large epicentral distances, and long site periods. Ground motions were categorized as follows: low, with A/V < 0.8 g/m/s; moderate, with 0.8 g/m/s < A/V < 1.2 g/m/s; and high, with A/V > 1.2 g/m/s. The categorization of ground motions is subjective, assuming that low A/V, intermediate A/V ratio, and high A/V ground motions correspond to low-, moderate-, and high-frequency contents, respectively.

The Table 1 and Figure 5 present original ground motion that a match with M and R nearest from the site with a Variant content frequency, Response spectra Figure 4-b is called as deterministic response spectra and is utilized as target spectrum to conduct the spectral matching to develop the new time history in soil site

Table 1. Original ground motion

No.	RSN	Ground motion	Mw	R(Km)	Acceleration (g)	Velocity (m/s)	A/V Ratio	Frequency
1	4040	Bam 03	6.6	1.7	0.8076609	58.49169	1.3808131	High Frequency
2	8164	Duzce 99	7.14	2.65	0.2822281	28.94847	0.9749327	Medium Frequency
3	1120	Kobe 95	6.9	1.47	0.6177107	120.6149	0.5121347	Low Frequency

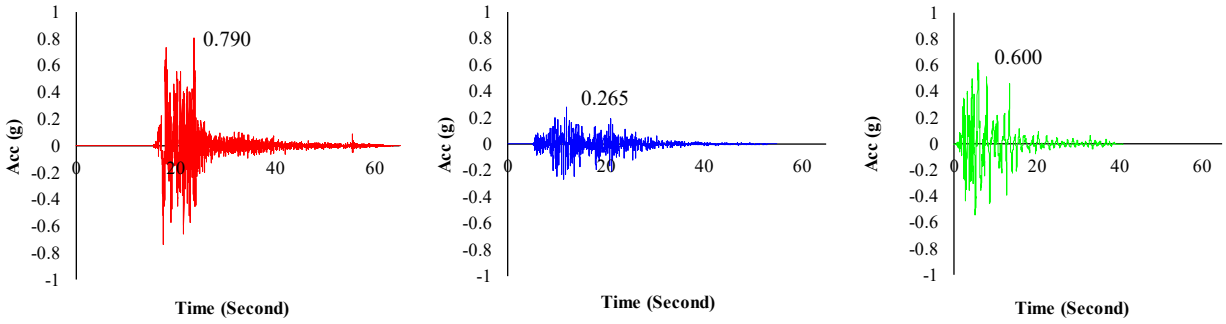

(a) High-Freq (b) Mid-Freq (c) Low-Freq

Figure 5. Original Time History Based on M = 6.6 and R=2 Km

The other basis to carried out the spectral matching is actual time history. The actual time history is a time history of measurement result. Time history of Bam 2003 in Iran that represents high Frequency (Figure 5-a), Duzce 1999 in Turki represents mid Frequency (Figure 5-b) and Kobe 1995 in Japan represents low frequency (Figure 5-c) above is the time history that used as other component to do the spectral matching beside the target spectrum. Response spectra of Bam 2003 (Figure 6-a), Duzce 1999 (Figure 6-b) and Kobe 1995 (Figure 6-c).

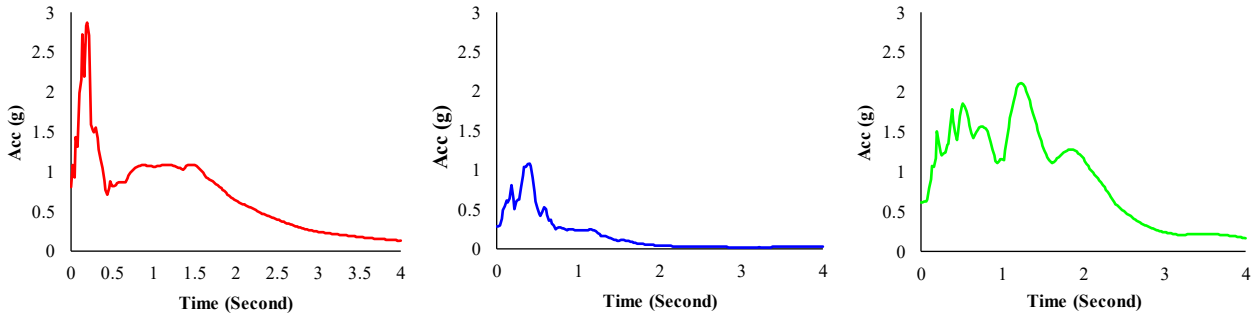

(a) High-Freq (b) Mid-Freq (c) Low-Freq

Figure 6. Response Spectra from Original Time history

4.3. Spectral Matching

Spectral matching is conducted between response spectra Figure 6 is matched to response spectra Figure 4-b. Result of spectral matching in form of the response spectra is in Figure 10-a. The matching time history result (Figure 7) whereas Figure 7-a represents high Frequency, Figure 7-b represents mid Frequency and Figure 7-c represents low Frequency.

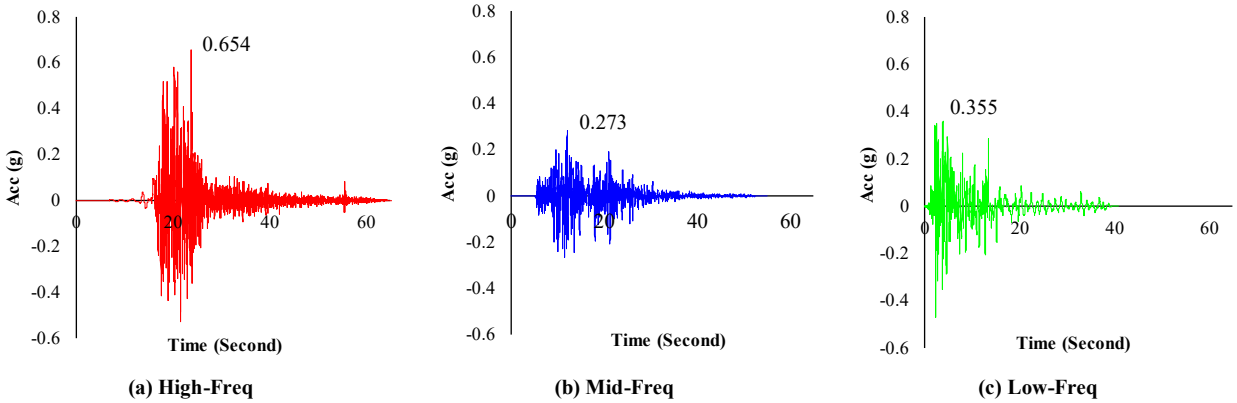

Figure 7. Time History Result of spectral matching

To obtain the earthquake wave at the soil surface as a time history, the earthquake wave depicted in Figure 7 must be propagated from the bedrock to the soil surface by ground response analysis. The analysis examines the vertical propagation of the shear wave from bedrock to the ground surface in a one-dimensional layered system. Bardet & Tobita (2001) [20] created a computer program for non-linear site response analysis of stratified soil deposits, employing the theory. The Equation employed for the analysis calculation is as follows:

$$\rho \frac{\partial^2 d}{\partial t^2} + \eta \frac{\partial d}{\partial t} = \frac{\partial \tau}{\partial z} \tag{11}$$

where ρ is the soil unit mass, d is the horizontal displacement, z is the depth, t is the time, τ is the shear stress, and η is a mass-proportional dumping coefficient. But in the study is utilized the DEEPSOIL program computer to propagate and find the earthquake wave in the soil surface, as inputted to DEEPSOIL N-SPT and Vs should be known (Figure 8).

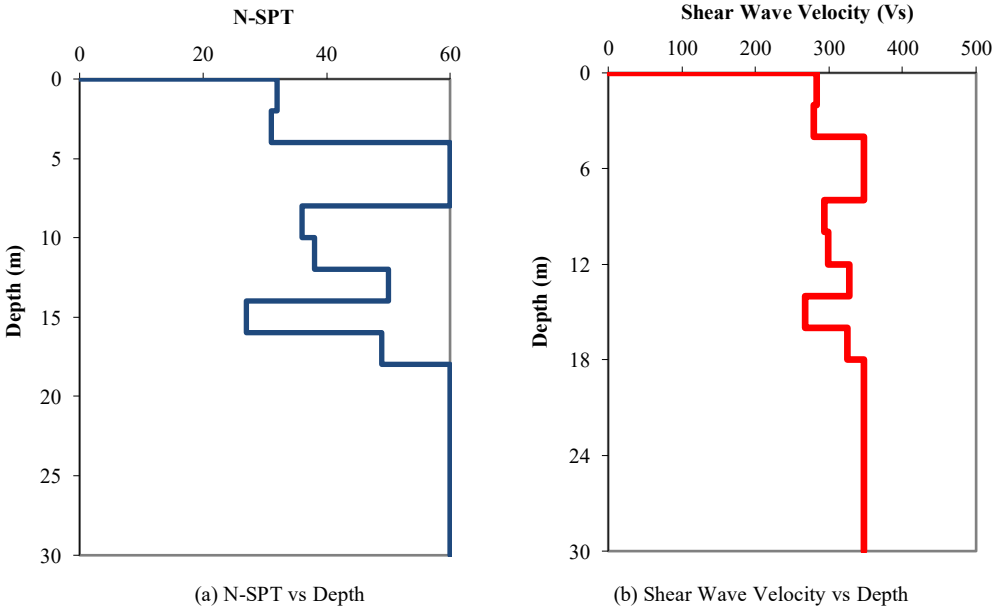

Figure 8. N-SPT and vs Depth

Figure 9, time history is designated as the deterministic time history (DSHA time history) because it is derived from the deterministic response spectrum and has undergone analysis of wave propagation through the ground layer. Due to the inelastic analysis conducted in the Yogyakarta, Indonesia region, it is subsequently aligned with the response spectrum according to The Risk-Targeted Maximum Considered Earthquake [21]. The spectral (Figure 10-b) and time history Figure 11 on surface after matching response spectra accordance The Risk-Targeted Maximum Considered Earthquake [21].

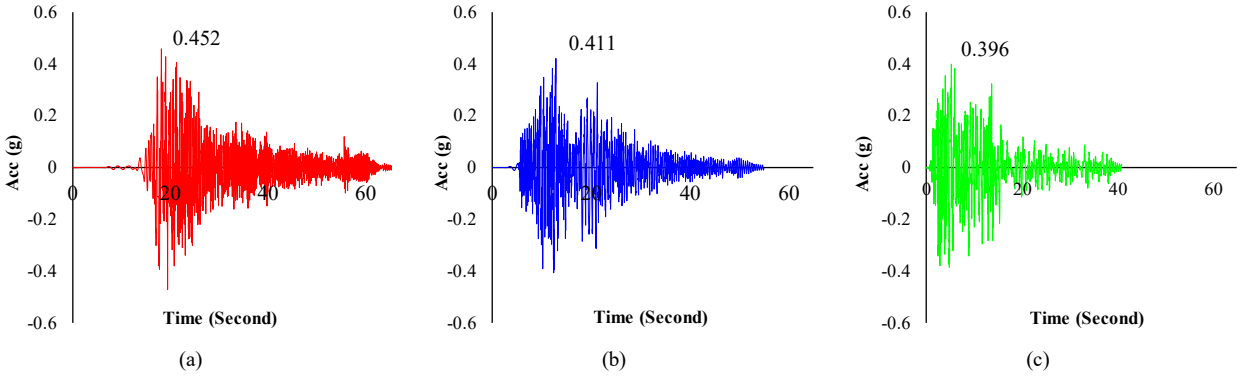

Figure 9. Time history at Surface based on Deterministic Analysis

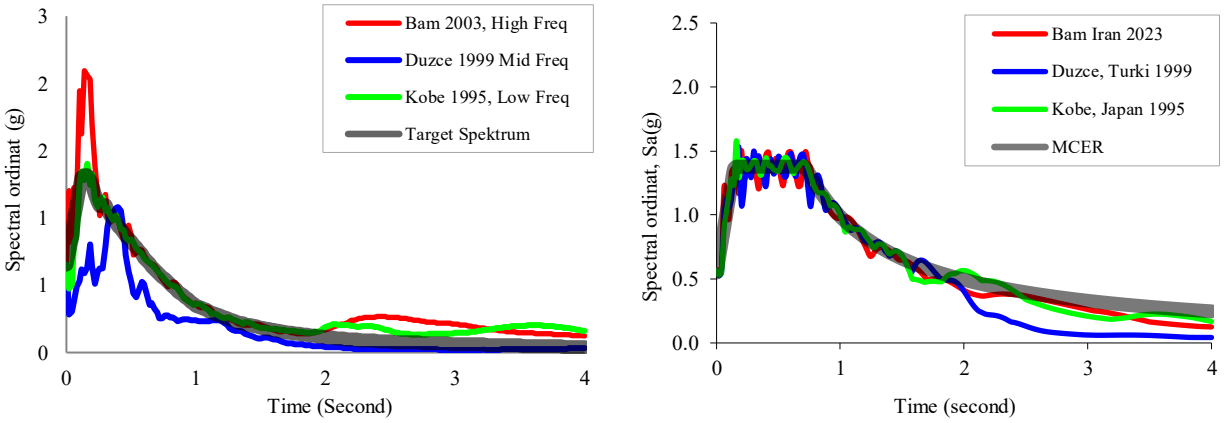

(a) Spectral Matching to Avg GMPE *(b) Spectral matching to MCE$_R$*

Figure 10. Result of spectral matching

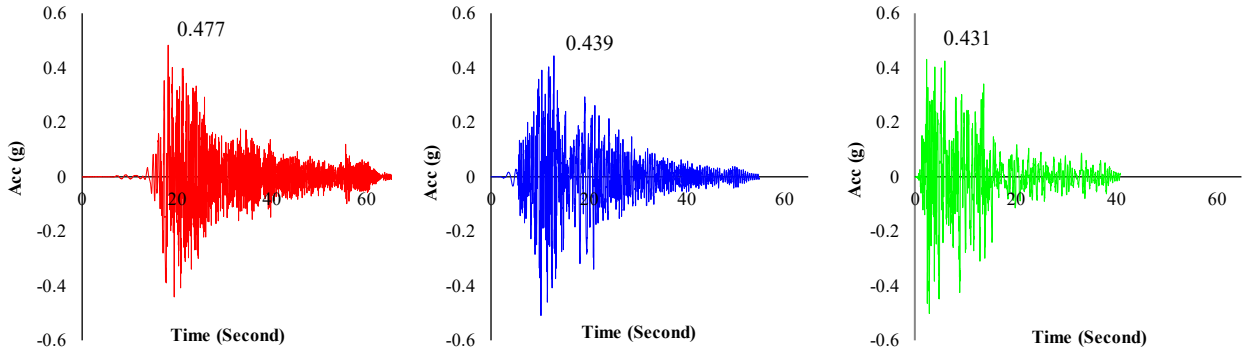

(a) High-Freq *(b) Mid-Freq* *(c) Low-Freq*

Figure 11. Time history Matching result to The Risk-Targeted Maximum Considered Earthquake (MCE$_R$)

5. Soil Structure Interaction

Soil Structure Interaction (SSI) is a physical phenomenon in which the structure fails to behave independently and behaves in connection with the soil when an external load is applied to the structure. In particular, the ground and the structures are greatly influenced by earthquakes, so this phenomenon is required as an essential consideration for seismic design. SSI can be divided mainly into two different methods. The first method is the Direct Method, which considers the ground and the structure as a complete system and models it like a structure using finite elements or finite differential methods. The second method is the Substructure Method, which treats the mechanical behavior of the soil as a single system with independent stiffness and damping. This study used the lumped parameter method as a simplified approach to model foundation vibrations. The soil parameters required to calculate the stiffness and damping values of the foundation are the N-SPT value, elastic modulus, foundation bearing capacity, soil specific gravity, Poisson's ratio, and shear wave velocity. All of these are obtained from soil investigations conducted at the building site using a single Borlog test point.

5.1. Vertical Vibrations

Soil pile analysis developed by Novak [22] for vertical vibrations of piles and piles under lateral and rocking motion are presented. In these procedures, the soil pile stiffness and damping have been evaluated for the system. A complete dynamic analysis can then be performed.

Novak [22] determined the variation of the amplitude and phase with (1) relative depth z/i, (2) slenderness ratio l/ro, (3) wave velocity ratio Vs/vc, (4) frequency ratio a, for v = 0.5, (5) density ratio ρ/ρρ = 0.7, which is typical of reinforced concrete piles, and (6) shear wave velocity ratios Vs = 1 and 10,000 that characterize floating and end-bearing piles, respectively. Internal damping of the pile has been neglected. These plots indicated that:

- The tip condition is particularly important in soft soils.
- It is only the upper part of a pile that undergoes significant displacement in which even a very long pile can vibrate almost as a rigid body.

The increase in the phase shift where visible is indicative of increased damping. In the design of pile-supported footings and structures, the stiffness and damping constants of the soil-pile system at the level of the pile head are needed. Having determined these quantities, the remaining procedure is the same as that for endbearing piles. The complex stiffness is equal to the force that produces a unit dynamic displacement of the pile head at a certain frequency. we obtain the complex stiffness as:

$$K_w = \frac{E_p A}{l} F_w(\Lambda) \tag{12}$$

where $F_w(\Lambda) = -\Lambda C(\Lambda) = F_w(\Lambda)_1 + iF_w(\Lambda)_2$.

The stiffness constant k, of one pile can be rewritten as:

$$k_w^1 = \frac{E_p A}{r_0} f_{w1} \tag{13}$$

where:

$$f_{w1} = \frac{F_w(\Lambda)_1}{l/r_0} \tag{14}$$

The constant of equivalent viscous damping of one pile is E_p, AFw, $(\Lambda)_2$, (lω), which can be written as:

$$c_w^1 = \frac{E_p A}{V_s} f_{w2} \tag{15}$$

where E_p is the elastic modulus of the foundation pile material, A is the area of the foundation pile, l is the length of the pile, k_w is the stiffness constant, r_o is the radius of the pile, w_c is the equivalent viscous damping constant and V_s is shear wave velocity.

5.2. Lateral Vibrations

Novak (1974) [23] had derived lateral stiffness and damping constants for single piles with soil modulus constant with depth. The considered (1) translation, Figure 12-a(a1), (2) rotation, Figure 12-a(b1), and (3) coupled rotation and translation. Novak & El-Sharnouby (1983) [24] extended these solutions to include parabolic variation of soil-shear modulus also. Equations 16 to 21 summarize the stiffness and damping coefficients and Table 2 lists values of constants used. Translation stiffness constant.

$$k_x^1 = \frac{E_p I_p}{r_0^3} (f_{x1}) \tag{16}$$

Translation damping constant,

$$c_x^1 = \frac{E_\rho I_\rho}{r_0^2 V_s} \left(f_{x_2}\right) \tag{17}$$

Rotation stiffness constant,

$$k_\phi^1 = \frac{E_\rho I_\rho}{r_0} \left(f_{\phi_1}\right) \tag{18}$$

Rotation damping constant,

$$c_\phi^1 = \frac{E_\rho I_\rho}{V_s} \left(f_{\phi_2}\right) \tag{19}$$

Cross-stiffness constant,

$$k_{x\phi}^{1} = \frac{E_\rho I_\rho}{r_0^2} f_{(x\phi_1)} \quad (20)$$

Cross-damping constant,

$$c_{x\phi}^{1} = \frac{E_\rho I_\rho}{r_0 V_s} f_{(x\phi_2)} \quad (21)$$

in which Ip moment of inertia of pile cross-section and Ep, Vs, Vc, r_o, f are Young's modulus of pile, shear wave velocity in soil, longitudinal wave velocity in pile, pile diameter, constants parameter, respectively.

5.3. Group Action Under Dynamic Loading

Piles are generally used in groups. The stiffness and damping of pile groups need be evaluated from considerations of group action. It is not correct to assume that group stiffness and damping are the simple sum of the stiffness and damping of individual piles. The extent of group action depends on the ratio of spacing to diameter of piles.

5.4. Vertical Vibrations

Novak & Grigg (1976) [25] proposed that the deflection factors of Poulos [26] for group action of statically loaded piles based on elastic analysis may also be applied to a pile group undergoing steady-state vibration. Therefore, stiffness of pile group k may be obtained from Equation 22:

$$k_w^g = \frac{\sum_1^n k_w^1}{\sum_1^n \alpha_A} \quad (22)$$

where n number of piles and α_A axial displacement interaction factor for a typical reference pile in the group relative to itself and to all other piles in the group, assuming the reference pile and all other piles carry the same load. The factor α_A is obtained from Figure 12-b. The equivalent geometric damping ratio for the group is given by:

$$c_w^g = \frac{\sum_1^n c_w^1}{\sum_1^n \alpha_A} \quad (23)$$

where is α_A is a *Interaction factor*.

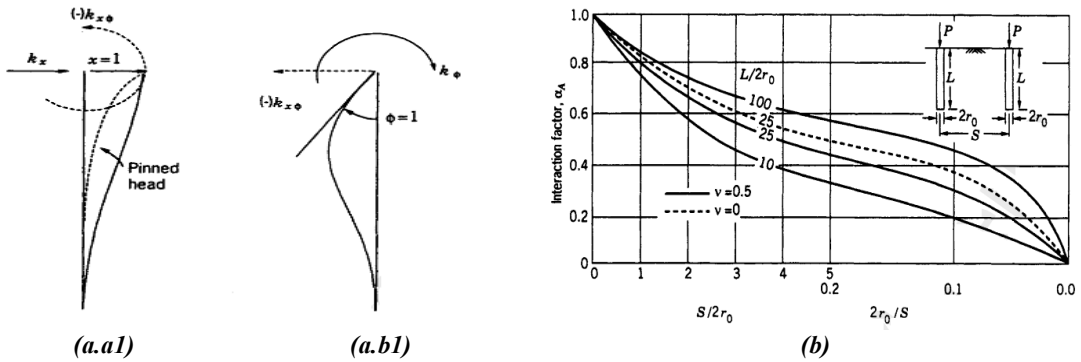

(a.a1) *(a.b1)* *(b)*

Figure 12. (a) Generation of lateral pile stiffness in individual directions: (a.a1) Horizontal, (a.b1) rotation (Novak & El-Sharnouby [24]); (b) Function of pile length and spacing (Poulos [26])

Novak & Beredugo (1972) [27] have developed expressions for calculating stiffness and geometric damping constants for embedded footings that can be applied to pile caps. These are added to the stiffness (k_w^f) and damping (c_w^f) values obtained in Equations 24 and 25. values due to side friction of the pile cap is expressed as (Prakash [28]):

$$k_w^f = G_s . h . \bar{S}_1 \quad (24)$$

$$c_w^f = h . r_0 . \bar{S}_2 \sqrt{G_s . \rho_s} \quad (25)$$

where h depth of embedment of the cap and r_o equivalent radius of the cap. G_s, and ρ_s are the shear modulus and total mass density of the backfill and $\bar{S}_1$ and $\bar{S}_2$ are constants and are 2.70 and 6.70, respectively.

5.5. Lateral Vibrations

In lateral vibrations, the stiffness and damping for groups of piles is given by:

$$k_x^g = \frac{\sum_1^n k_x^1}{\sum_1^n \alpha_L} \quad (26)$$

$$c_x^g = \frac{\sum_1^n c_x^1}{\sum_1^n \alpha_L} \quad (27)$$

where α_L displacement factor for lateral translation and may be adopted from Figure 13.

Again, as for vertical vibrations, the spring costant k_x^f and damping c_x^f due to pile cap translation are, respectively:

$$k_x^f = G_s . h . \bar{S}_{x1} \quad (28)$$

$$c_x^f = h . r_0 . \bar{S}_{x2} \sqrt{G_s . \rho_s} \quad (29)$$

where h depth of embedment, r_o equivalent radius of the cap, G_s the shear modulus, ρ_s total mass density of the backfill and $\bar{S}x_1$, $\bar{S}x_2$ With a Poisson's ratio of 0.4, the values are 4.1 and 10.6, respectively.

The total stiffness and total damping values are sums of Equations 26 to 29, respectively, as:

$$\text{Total } k_x^g = k_x^g + k_x^f \quad (30)$$

$$\text{Total } c_x^g = c_x^g + c_x^f \quad (31)$$

6. Building Information and Parameters Used

The Hotel structure in Yogyakarta, Indonesia is subjected to structural study. The study was conducted to assess the structural response of the Structure Hotel (Figures 13 and 14) to the earthquake acceleration wave, represented by the time history in Figures 11. The Structural Analysis Program, Ruaumoko 3D, was used to simulate shaking on the structure.

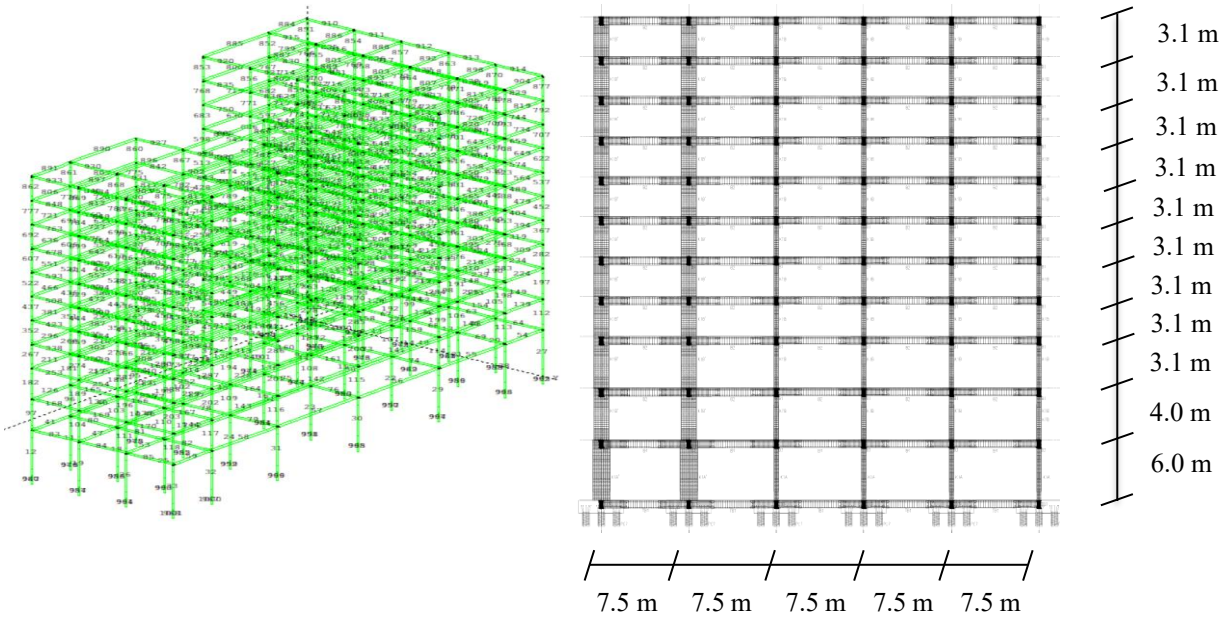

(a) Structure modeling using Ruaumoko 3D **(b) Section of structure Grid 3**

Figure 13. 3D Model and Structure section

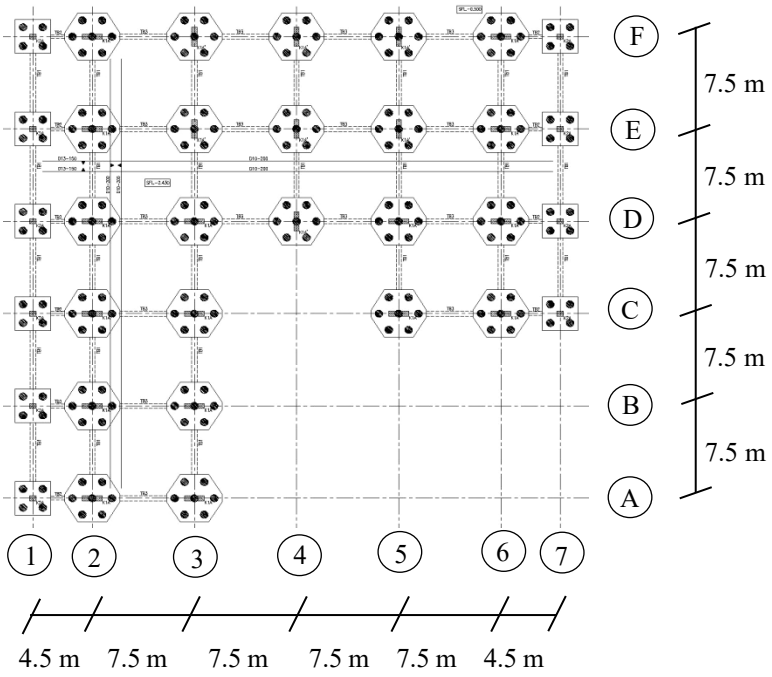

Figure 14. Foundation Layout

Base flexibility is introduced by using a series of springs at the end of the pile foundation. The spring constant is calculated using the concept of dynamic stiffness (impedance function) as presented by Prakash [28]. This approach considers the influence of mass and damping. The stiffness and damping of the soil-foundation system (K and C) are presented in Table 2. F1 represent number of pile are four where is location on grid 1/A, 1/B, 1/C, 1/D, 1/E, 1/F, 7/C, 7/D, 7/E, 7/F and F2 represent number of pile are seven where is location on grid 2/A, 2/B, 2/C, 2/D, 2/E, 2/F, 2/C, 2/D, 2/E, 2/F, 3/A, 3/B, 3/C, 3/D, 3/E, 3/F, 3/C, 3/D, 3/E, 3/F, 4/D, 4/E, 4/F, 5/C, 5/D, 5/E, 5/F, 6/C, 6/D, 6/E, 6/F.

Table 2. Stiffness and Damping Foundation

No.	Code	Vertical spring constant		Horizontal spring constant		Rocking constant	
		Stiffness and Damping		Stiffness and Damping		Stiffness and Damping	
		∑Kwg	∑Cwg	Kx	Cx	Køg	Cøg
		(kN/m)	(t-sec/m)	(kN/m)	(t-sec/m)	(kN/m)	(t-sec/m)
1	F1	37062.05899	4643.753541	64561.9478	2298.906454	883209465.7	18358247.84
2	F2	38061.51016	5529.025511	68620.9236	3193.477346	1718556068	69448983.98

7. Structural Analysis Result

The analysis results indicate that the Fundamental period for the fixed support is 2.4 seconds, whereas for the flexible Support, it is 2.8 seconds. This discrepancy is typical, as the flexible support accounts for surrounding soil conditions and the deformation effects of the soil. Deterministic analysis derives the subsequent responses of structures subjected to earthquake loads characterized by high, medium, and low frequency content. In the result of analysis with figure, it is stated that the red line represents ground motion with high-frequency content, the blue line represents ground motion with medium-frequency content, and the green line represents ground motion with low-frequency content, while the solid line represents a structure with fixed supports and the dashed line represents a structure with flexible supports.

7.1. Displacement and Drift Ratio

The structural response shows displacement and drift ratio, with the analysis results limited to the X direction solely due to writing constraints. The difference seen in the analysis results shows that flexible support displacement more than fixed support. This effect can be seen in Figure 15-a, where the dashed line indicates a higher value compared to the solid line, and ground motion with high-frequency content are more sensitive to structural response compared to low-frequency ground motion, as can be seen in the observed deviations. The maximum deviation occurs at 0.6357 m on the roof floor (Figure 15-a). Additionally, the largest drift ratio occurs during high-frequency content earthquake vibrations, specifically on the 4th floor, with a drift ratio of 0.0320 (Figure 15-b).

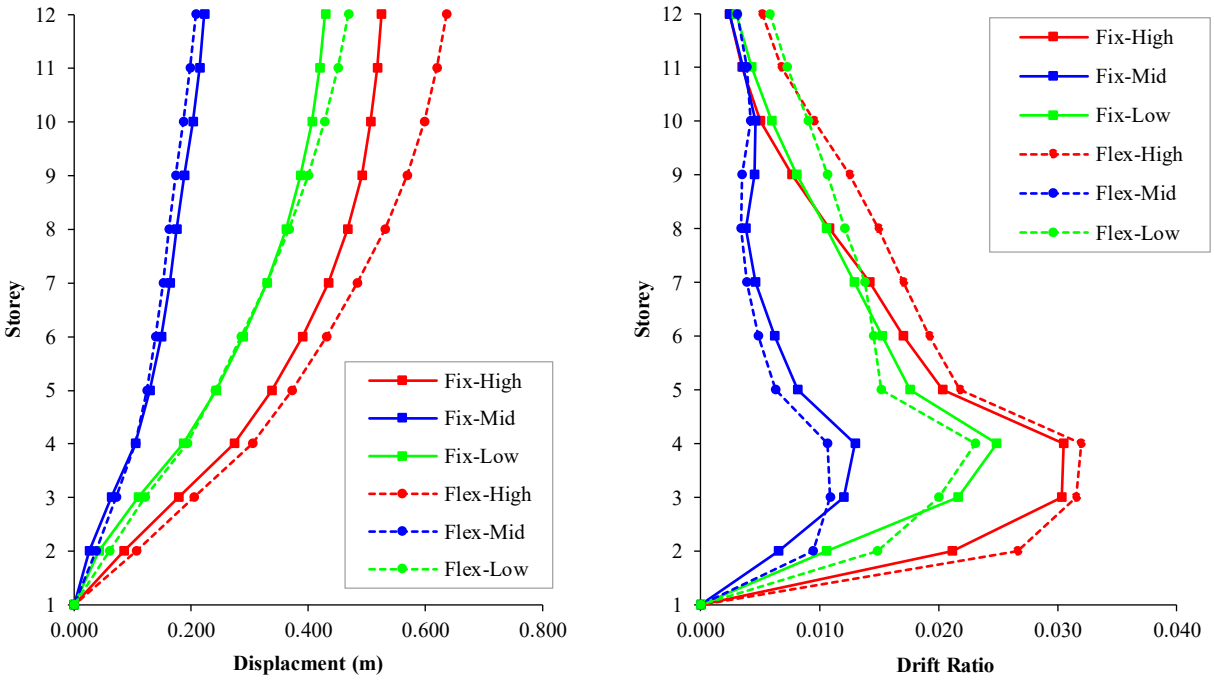

(a) Displacement *(b) Drift ratio*

Figure 15. Displacement and Drift Ratio

7.2. Beam's Curvature dan Plastic Hinge Rotation

In performance-based seismic design (PBSD), plastic hinge rotation is often used as a criterion for structural performance. Plastic hinge rotation is obtained from the product of curvature (rad/m) and the length of the plastic hinge (the length of the plastic hinge is determined using the Paulay and Priestley formula 1992 0.08L+0.022.db.fy). The figure below shows the curvature distribution of the beam due to ground motion, as determined by deterministic analysis. It can be seen in the picture that the curvature distribution at all levels resembles the drift ratio distribution. It can be seen that the rotation of the plastic hinge due to the deterministic earthquake results on flexible supports yields greater results compared to those on structures with fixed supports (Figure 16), while ground motion with high, medium, and low frequency content shows that the rotation of the plastic hinge at high frequency AGMTH is greater at 0.004651, and medium frequency content is greater at 0.00309 compared to low frequency content at 0.001494. These results indicate a structural response that is sensitive to high-frequency AGMTH.

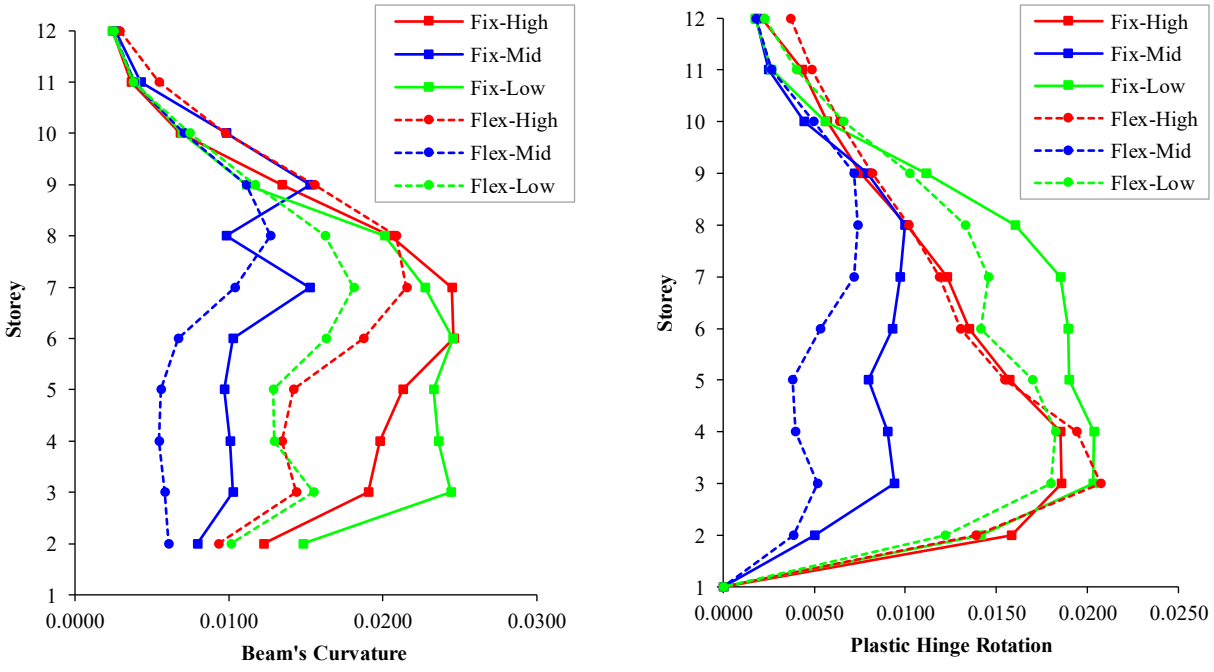

(a) Beam curvature *(b) Plastic hinge rotation*

Figure 16. Beam curvature and Plastic hinge rotation

7.3. Beam Element Stiffness History

The building structure's excessive number of beams serves as an example of the historical rigidity of a beam. The chosen beam code is 135 (3rd floor grid 5). The stiffness of the element will vary based on the level of structural response. Figure 17 (Fixed support) and Figure 18 (flexible support) illustrates the stiffness history of element 135. The average stiffness of element 135, as determined by the earthquake data presented in the figure, shows that structures with fixed supports exhibit higher average values compared to structures with flexible supports. For example, for ground motion with high-frequency content, 71.08% of fixed supports and 70.39% of flexible supports were observed. The medium-frequency content surpasses the low and high frequency content, which also stands at 91.85%. This result indicates a structural response that is highly sensitive to low-frequency of ground motion.

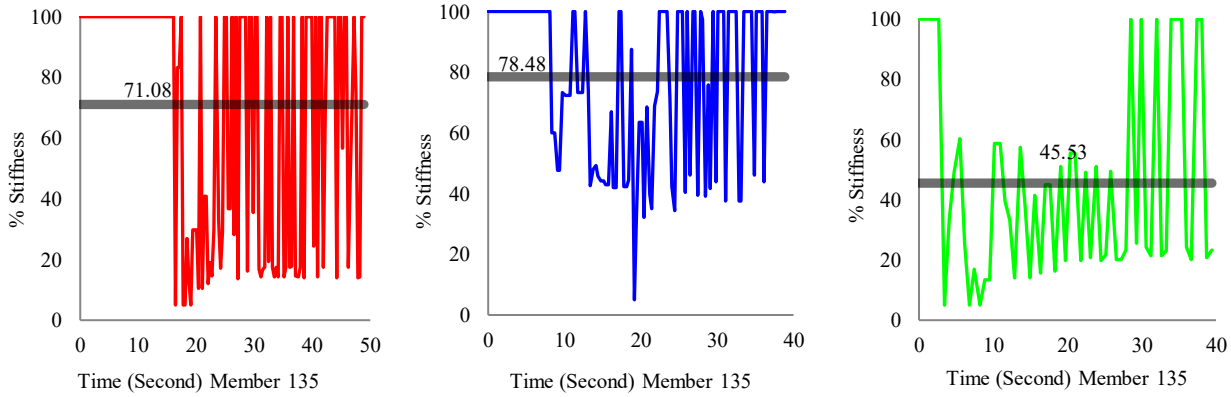

(a) High-Freq *(b) Mid-Freq* *(c) Low-Freq*

Figure 17. Stiffness History of Beam 135 Fixed Support

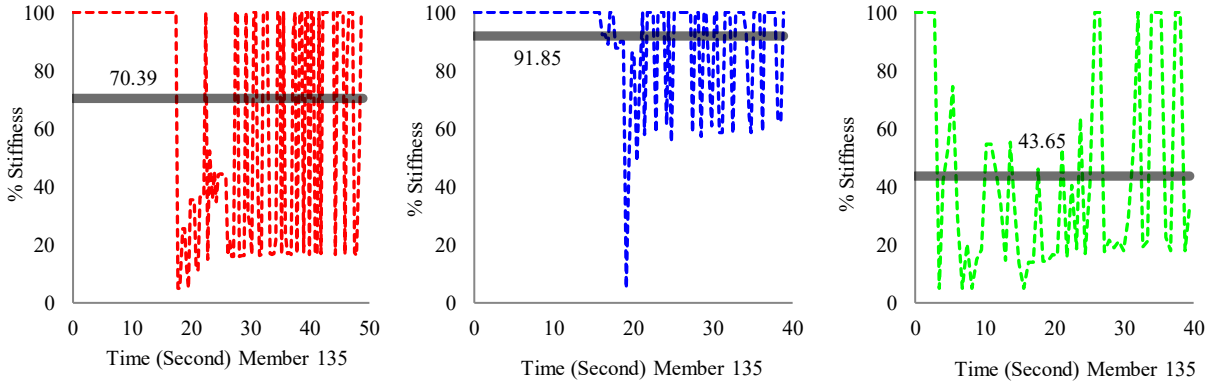

(a) High-Freq *(b) Mid-Freq* *(c) Low-Freq*

Figure 18. Stiffness History of Beam 135 Flexible Support

7.4. Energy Dissipation

Civil engineering rarely discusses energy. Physics divides energy into different types: kinetic energy comes from movement; strain energy is created when materials change shape; viscous energy is caused by friction between solids and liquids; and hysteretic energy relates to how structural elements respond when they are not perfectly elastic. Input energy refers to the energy introduced or absorbed in the structure as a result of seismic vibrations. The mathematical balance between energy input and its distribution includes kinetic, viscous, strain, and hysteretic components. Figure 19 shows how energy from predictable earthquakes with fixed support has been balanced over time with how that energy spreads out and is lost. The figure shows that at the end of the loading phase, the actual energy input remains substantial, as evidenced by the continuous increase in energy input, which is reflected in the energy line that remains stretched rather than flat. Energy input with a Fixed support, as illustrated in Figure 19, shows a higher value compared to the flexible support structure (Figure 20), with a relatively small increase toward the end of the loading, as evidenced by the mostly flat energy input line. The result shows that the energy from a strong earthquake with a flexible support is much higher than the energy from a fixed support. The evidence also indicates that the fixed support will produce a more significant response or damage compared to the flexible support.

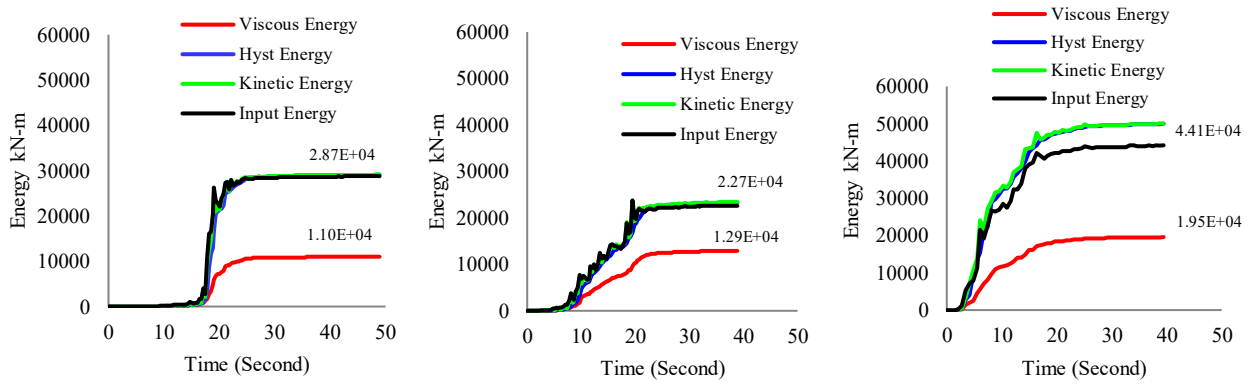

(a) High-Freq *(b) Mid-Freq* *(c) Low-Freq*

Figure 19. Energy Dissipation Fixed Support

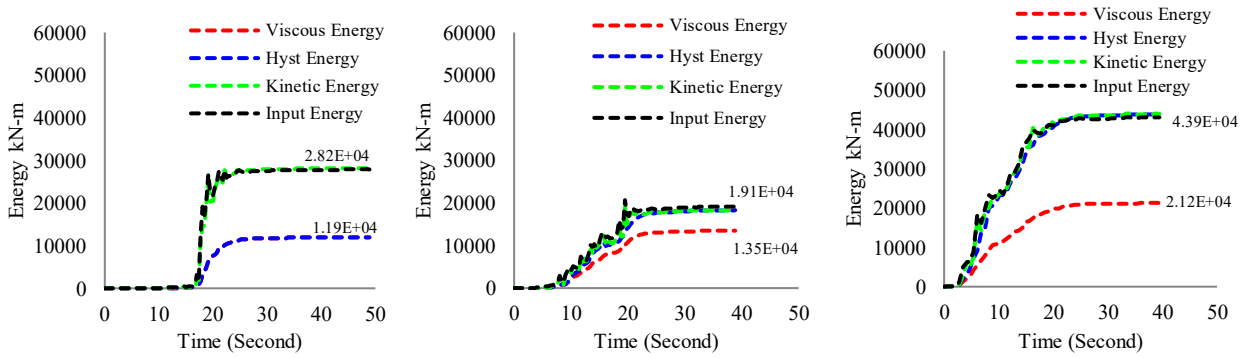

(a) High-Freq *(b) Mid-Freq* *(c) Low-Freq*

Figure 20. Energy Dissipation Flexible Support

7.5. Beam Hysteretic Loops

Hysteretic loops of the beam used Takeda's hysteresis model initially uses uncracked stiffness, then after cracking, the stiffness decreases, which is consistent with the behavior of concrete elements. Hysteretic loops with an Artificial Ground motion Time History based on Deterministic seismic hazard analysis are presented in Figure 21. The chosen beam code is 223 (4th floor grid 5), structure with fixed support and 22 structure with flexible support (see Figure 22). The hysteretic loops represent graphs with horizontal force as the ordinate and horizontal deviation as the abscissa. The horizontal force P(tf) represents the ordinate, while the curvature serves as the abscissa. The hysteretic shape can be nearly symmetrical at times, while at other times it is not. Researchers indicate that the hysteretic area reflects the element's capacity to absorb and release energy. A bigger hysteretic area indicates more energy absorption capacity of the structure, which is advantageous. The figure indicates that the hysteretic loop in columns subjected to high-frequency earthquake vibrations (Figure 21-a) is broader than that associated with lower-frequency earthquake vibrations. It can be deduced that the beam's structural reaction has become inelastic, indicating a reduction in element stiffness.

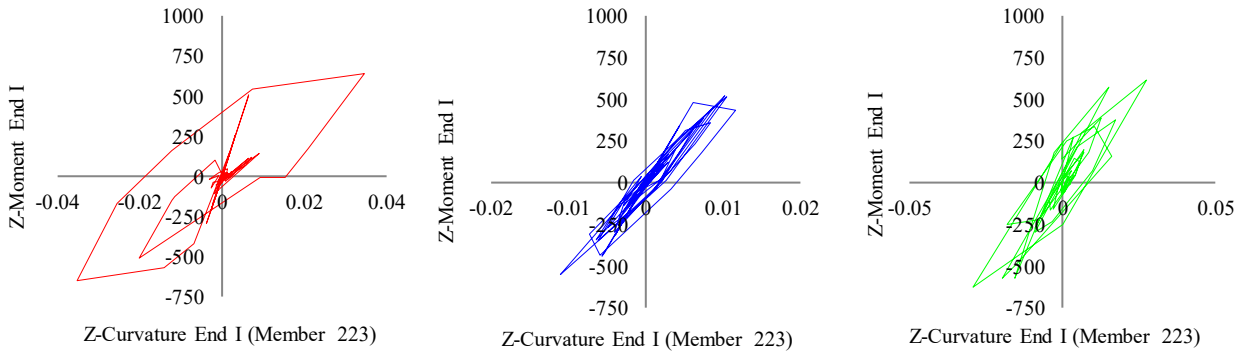

(a) High-Freq *(b) Mid-Freq* *(c) Low-Freq*

Figure 21. Hysteretic Loops Beam (Member 223) Fixed Support

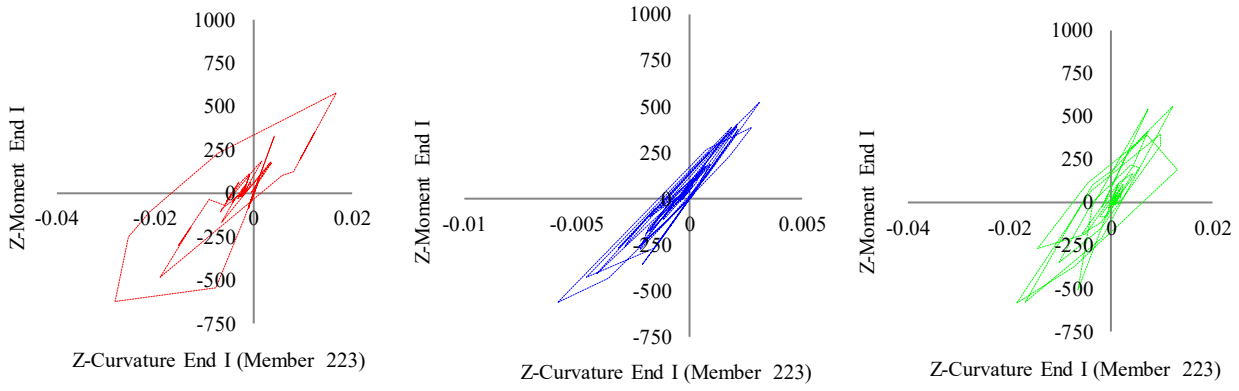

(a) High-Freq *(b) Mid-Freq* *(c) Low-Freq*

Figure 22. Hysteretic Loops Beam (Member 223) Flexible Support

7.6. Damage Index

The Ruaumoko 3D program automatically generates the damage index formula, which follows Park and Ang (1985) [29]. A numerical "damage index" can quantify damage in structural analysis and design. Damage indices can come from a number of places, such as the results of a nonlinear dynamic analysis or the way a structure behaved during an earthquake. Usually, damage indices are number-based numbers that range from 0 (which means the structure is not damaged) to 1 (which means it has collapsed), with values in between showing different levels of damage. The most significant result would be the precise assessment of repercussions associated with the projected damage index for a hypothetical earthquake. Figure 17 illustrates how the artificial ground motion time history, which is based on deterministic seismic hazard analysis, provides the damage index. Therefore, it can be said that the Fixed support not always higher than flexible support (Figure 23-b). High and low frequency of ground motion gives a greater damage index compared to other time histories with mid frequency content.

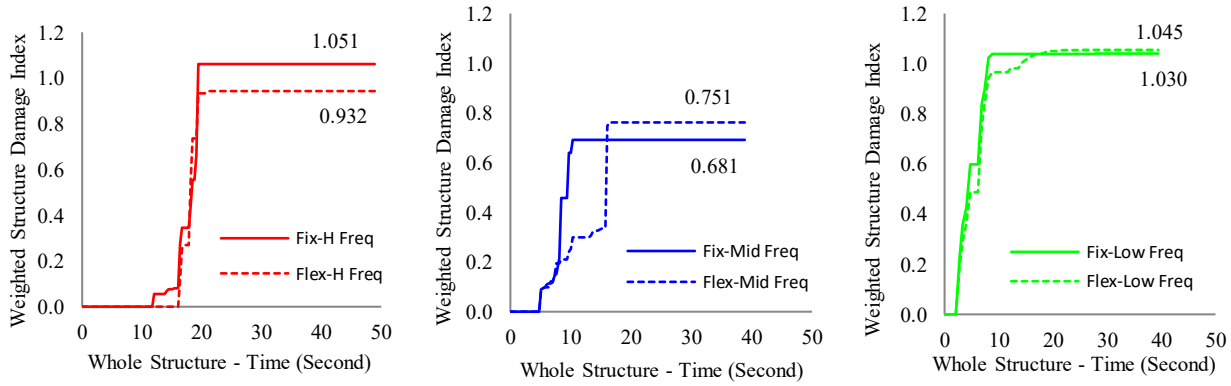

(a) High-Freq *(b) Mid-Freq* *(c) Low-Freq*

Figure 23. Global Damage Indices

8. Discussion

The analysis results indicate that the Fundamental period for the fixed support is 2.4 seconds, whereas for the flexible Support, it is 2.8 seconds ($\tilde{T}$/T=1.16). Generally, flexible support will increase the fundamental period of the structure by 1.1 to 1.5 times, as indicated by the National Institute of Standards and Technology (NIST GCR 12-917-21). This phenomenon occurs because the foundation rests on deformable soil media, ratio $\tilde{T}$/T depending on the specific characteristics of the soil and structure.

Displacement and drift ratio at fixed supports subjected to high-frequency ground motion are lower than those at flexible supports, which also exhibit greater responsiveness to medium and low-frequency content. This demonstrates that flexible supports are more sensitive to displacement and drift ratios. The analysis of the displacement and drift ratio indicates that the displacement resulting from earthquakes with high frequency content is 635 mm, with intermediate frequency at 207 mm, and low frequency at 467 mm. This demonstrates that the structure is highly responsive to ground motion with high frequency content. The maximum displacement of 0.6357m and a building height of 37.9m, the global drift ratio is obtained as 1.6 (exceeding 1.5 but less than 2.5), according to the structural performance criteria outlined in Vision 2000, this is classified as Near Collapse (NC), indicating that the building structure is nearing failure.

Beam curvature and plastic hinge rotation at the fixed support exhibit greater values in high-frequency ground motion compared to the flexible support, as well as in middle and low-frequency content. This suggests that the fixed support is more responsive to the occurring beam curvature and plastic hinge rotation. The analysis of beam curvature and plastic hinge rotation indicates that the curvature resulting from high-frequency earthquakes is 0.0267, medium frequency is 0.00952, and low frequency is 0.0235, demonstrating that the structure is highly responsive to ground motion with high-frequency content.

Beam stiffness analysis results indicate that the fixed support exhibits a greater value in response to high-frequency ground motion compared to the flexible support, as well as at medium and low frequencies. This demonstrates that the fixed pedestal is more sensitive to the beam stiffness variations. The beam stiffness analysis results indicate that the stiffness attributable to high-frequency earthquakes is 70.39%, to intermediate frequency is 91.85%, and to low frequency is 43.65%. This demonstrates that the structure is highly responsive to ground motion with high-frequency content.

The energy dissipation analysis results indicate that the fixed support exhibits a greater value than the flexible support for high, medium, and low frequency content ground motion, demonstrating that the fixed support is more adept at energy dissipation. Similarly, the results of the energy dissipation analysis indicate that the energy content from high-frequency earthquakes is greater than that from intermediate frequencies, while low-frequency content is even higher. This suggests that the structure is highly responsive to ground motion with high-frequency content.

Hysteretic loop study results indicate that the fixed support exhibits a greater response to high-frequency ground motion compared to the flexible support, as well as in the mid and low-frequency ranges, suggesting that the fixed support is more reactive to the occurring hysteretic loops. The results of the hysteretic loop analysis suggest that the response of the structure to high-frequency ground motion is significantly stronger than its response to medium and low-frequency content during earthquakes.

The damage index study results reveal that the fixed support exhibits a larger value than the flexible support across high, medium, and low frequency content, suggesting that the fixed support is more susceptible to the damage index fluctuations. The damage index research reveals that the damage index for earthquakes with high frequency content is 0.932, for medium frequency it is 0.751, and for low frequency it is 1.04, indicating that the structure is very responsive to ground motion with low frequency content. According to the maximum damage index of 1.051, which exceeds one, and following the damage index categorization by Park & Ang (1985) [29], the structure is classified as collapsed. When comparing the performance levels of structures based on displacement that occurs near collapse with the damage index at collapse, there is a difference in performance levels, although not very significant. It would therefore be very intriguing to determine the correlation between performance levels based on different methods.

9. Conclusion

The analysis results at the site located 2 km from the fault and the 6.6 Mw earthquake scenario indicate that deterministic ground motion with high-frequency content leads to structural collapse. The analysis results indicate that the fundamental period for the fixed support is 2.4 seconds, whereas for the flexible support, it is 2.8 seconds. Likewise, displacement and drift ratio at fixed supports subjected to high-frequency ground motion are lower than those at flexible supports. Beam curvature and plastic hinge rotation at the fixed support exhibit greater values in high-frequency ground motion compared to the flexible support, whereas the energy dissipation analysis results indicate that the fixed support exhibits a greater value than the flexible support. Finally, the damage index study results reveal that the fixed support exhibits a larger value than the flexible support. The topic of inelastic response is of great interest for further research, especially comparing it with probabilistic, deterministic, and Indonesian regulation earthquake motions and also the variation of the number of stories in the building, in order to find out which earthquake scenario has the greatest effect on the structure.

10. Declarations

10.1. Author Contributions

Conceptualization, W.P. and P.P.; methodology, Y.M.; software, P.P.; validation, P.P., W.P., and L.M.; formal analysis, P.P.; investigation, P.P.; resources, L.M.; data curation, W.P.; writing—original draft preparation, P.P.; writing—review and editing, P.P. and W.P.; visualization, Y.M.; supervision, W.P.; project administration, P.P.; funding acquisition, P.P. All authors have read and agreed to the published version of the manuscript.

10.2. Data Availability Statement

The data presented in this study are available in the article.

10.3. Funding

The authors received no financial support for the research, authorship, and/or publication of this article.

10.4. Acknowledgements

The author gratefully acknowledgement to soil mechanics laboratory Islamic University of Indonesia, that has supported this research in encouragement

10.5. Conflicts of Interest

The authors declare no conflict of interest.

11. References

[1] Husein, S., Karnawati, D., Pramumijoyo, S., & Ratdomopurbo, A. (2007). Geological Control of Land Response in the Yogyakarta Earthquake of May 27, 2006: efforts to create a micro-zoning map in the Bantul area. Proceeding Seminar Nasional 2007 Geotechnics for Earthquake Engineering, 25-28 June, 2007, Thessaloniki, Greece. (In Indonesian).

[2] Hanindya, K. A., Makrup, L., Widodo, & Paulus, R. (2023). Deterministic Seismic Hazard Analysis to Determine Liquefaction Potential Due to Earthquake. Civil Engineering Journal (Iran), 9(5), 1203–1216. doi:10.28991/CEJ-2023-09-05-012.

[3] Widodo. (1995). Rocking Of Multi Storey Building. Ph.D. Thesis, University of Canterbury, Christchurch, New Zealand.

[4] Widodo P., & Mushthofa, M. (2023) Contibution of normalized Hysteritic Energy to damage Index in inelastic response of SDOF Structure due to earthquake. Journal Teknisia, 28(01), 055-069. (In Indonesian).

[5] Zhang, X., & Far, H. (2024). Beneficial and detrimental impacts of soil-structure interaction on seismic response of high-rise buildings. Advances in Structural Engineering, 27(11), 1862–1886. doi:10.1177/13694332241255747.

[6] Bradley, B. A. (2025). Seismic Hazard with Deterministic Maximum Limits: Considerations in a New Zealand-Specific Context. Bulletin of the New Zealand Society for Earthquake Engineering, 58(1), 1–10. doi:10.5459/bnzsee.1706.

[7] Pranowo, Makrup, L., Pawirodikromo, W., & Muntafi, Y. (2024). Comparison of Structural Response Utilizing Probabilistic Seismic Hazard Analysis and Design Spectral Ground Motion. Civil Engineering Journal, 10, 235–251. doi:10.28991/cej-sp2024-010-012.

[8] Ricci, A., Romanelli, F., Vaccari, F., Boncio, P., Venisti, N., Faraone, C., Vessia, G., & Panza, G. F. (2025). Comparison between the Neo-deterministic Seismic Hazard and FEM approach to assessing 2D local seismic response at Chieti's city site (Abruzzo, Italy). Engineering Geology, 347. doi:10.1016/j.enggeo.2024.107891.

[9] Campbell, K. W., & Bozorgnia, Y. (2003). Updated near-source ground-motion (attenuation) relations for the horizontal and vertical components of peak ground acceleration and acceleration response spectra. Bulletin of the Seismological Society of America, 93(1), 314-331. doi:10.1785/0120020029.

[10] Sadigh, K., Chang, C. Y., Egan, J. A., Makdisi, F., & Youngs, R. R. (1997). Attenuation relationships for shallow crustal earthquakes based on California strong motion data. Seismological Research Letters, 68(1), 180–189. doi:10.1785/gssrl.68.1.180.

[11] Chiou, B.-J., & Youngs, R. R. (2008). An NGA Model for the Average Horizontal Component of Peak Ground Motion and Response Spectra. Earthquake Spectra, 24(1), 173–215. doi:10.1193/1.2894832.

[12] Zhao, J. X., Zhang, J., Asano, A., Ohno, Y., Oouchi, T., Takahashi, T., Ogawa, H., Irikura, K., Thio, H. K., Somerville, P. G., Fukushima, Y., & Fukushima, Y. (2006). Attenuation relations of strong ground motion in Japan using site classification based on predominant period. Bulletin of the Seismological Society of America, 96(3), 898–913. doi:10.1785/0120050122.

[13] Kanno T., Narita A., Morikawa N., Fujiwara H., Fukushima Y. (2006). A new attenuation relation for strong ground motion in Japan based on recorded data. Bulletin of the Seismological Society of America, 96, 879–889.

[14] Nikolaou, A. S. (1998). A GIS platform for earthquake risk analysis. Ph.D. Thesis, State University of New York at Buffalo, Buffalo, United States.

[15] PuSGeN. (2022). Indonesia's Earthquake Hazard Deaggregation Map for Earthquake-Resistant Infrastructure Planning and Evaluation. National Earthquake Study Center, The Ministry of Public Works and Housing, Jakarta, Indonesia.

[16] Youngs, R. R., & Coppersmith, K. J. (1986). Implications of fault slip rates and earthquake recurrence models to probabilistic seismic hazard estimates. International Journal of Rock Mechanics and Mining Sciences & Geomechanics Abstracts, 23(4), 125. doi:10.1016/0148-9062(86)90651-0.

[17] Garg, R., Vemuri, J. P., & Subramaniam, K. V. L. (2019). Correlating peak ground A/V ratio with ground motion frequency content. Lecture Notes in Civil Engineering, 12, 69–80. doi:10.1007/978-981-13-0365-4_6.

[18] Tso, W. K., Zhu, T. J., & Heidebrecht, A. C. (1992). Engineering implication of ground motion A/V ratio. Soil Dynamics and Earthquake Engineering, 11(3), 133–144. doi:10.1016/0267-7261(92)90027-B.

[19] Sawada, T., Hirao, K., Yamamoto, H., & Tsujihara, O. (1992). Relation between maximum amplitude ratio and spectral parameters of earthquake ground motion. Tenth World Conference of Earthquake Engineering, 19-24 July, 1992, Madrid, Spain.

[20] Bardet J. P., Tobita T. (2001). NERA. A computer program for nonlinear earthquake site response analyses of layered Soil Deposits. Los Angeles. University of Southern California, California, United States.

[21] SNI 1726-2019. (2019). Earthquake Resistance Planning Procedures for Building and Non-Building Structures. Badan Standarisasi Nasional (BSN), Jakarta, Indonesia. (In Indonesian).

[22] Novak, M. (1977). Vertical Vibration of Floating Piles. Journal of the Engineering Mechanics Division, 103(1), 153–168. doi:10.1061/jmcea3.0002201.

[23] Novak, M. (1974). Dynamic Stiffness and Damping of Piles. Canadian Geotechnical Journal, 11(4), 574–598. doi:10.1139/t74-059.

[24] Novak, M., & El Sharnouby, B. (1983). Stiffness Constants of Single Piles. Journal of Geotechnical Engineering, 109(7), 961–974. doi:10.1061/(asce)0733-9410(1983)109:7(961).

[25] Novak, M., & F.Grigg, R. (1976). Dynamic experiments with small pile foundations. Canadian Geotechnical Journal, 13(4), 372–385. doi:10.1139/t76-039.

[26] Poulos, H. G. (1968). Analysis of the Settlement of Pile Groups. Géotechnique, 18(4), 449–471. doi:10.1680/geot.1968.18.4.449.

[27] Beredugo, Y. O., & Novak, M. (1972). Coupled Horizontal and Rocking Vibration of Embedded Footings. Canadian Geotechnical Journal, 9(4), 477–497. doi:10.1139/t72-046.

[28] Prakash, S., (1989) Foundation for Dynamic Load. John Wiley and Sons, Hoboken, United States.

[29] Park, Y., & Ang, A. H.-S. (1985). Mechanistic Seismic Damage Model for Reinforced Concrete. Journal of Structural Engineering, 111(4), 722–739. doi:10.1061/(asce)0733-9445(1985)111:4(722).